First principles investigation of spin-orbit coupling driven magnetism of the $3d$-$5d$ double-perovskite (Sr/Ca)$_2$FeIrO$_6$

Roumita Roy and Sudipta Kanungo[*]

School of Physical Sciences, Indian Institute of Technology Goa, 403401 Goa, India

The interplay of spin-orbit coupling (SOC) with the other energy scales gives rise to various novel and interesting quantum phenomena in the Ir based double perovskites. In recent findings the double-perovskites Sr$_2$FeIrO$_6$ (SFIO) and Ca$_2$FeIrO$_6$ (CFIO) have been reported to fall under the category of a SOC driven antiferromagnetic (AFM) Mott insulator. Using density functional theory based first principles calculations, we have performed a comparative electronic structure investigation of these compounds. We reveal the microscopic origin of the difference in the AFM transition temperature observed in the experiments through the calculated exchange interactions and the Wannier functions. We addressed the role of SOC in dictating the ground state properties of these two compounds. Although both of the compounds are isoelectronic and isovalent, however, the effective strength and the impact of SOC is very different and nonmonotonic in these compounds, due to the delicate balance with the other energy scales. Our study advances the understanding of the nontrivial role of SOC in driving ground state magnetic properties of the Ir based oxides in general and explores the opportunities for further designing of the SOC driven quantum phases.

I. INTRODUCTION

The double-perovskite family with a chemical formula of A$_2$BB$'$O$_6$ is widely studied, because of the rich physics it promises. The presence of two transition metals at sites B and B$'$ is responsible for introducing the interplay of different energy scales involved in the problem. Dealing with this competition might be difficult due to induced complexity, nevertheless this complexity gives this family its unadulterated fame due to various emergent phenomena such as giant magnetoresistance [1], metallicity [2], half-metallicity [3], Dirac-Mott insulator [4], Kitaev spin liquid [5], and many more.

In this context the $3d$-$5d$ combination of the transition metals in the double perovskite will be very interesting. Due to the huge difference in the spatial extensions, the former has a strong electronic correlation effect compared to the latter. On the other hand, SOC is a relativistic phenomena which originates due to the interaction of the intrinsic spin angular momentum of the electron with the orbital angular momentum embedded into the lattice. The strength of the SOC is an atomistic property, which is directly proportional to the fourth power of atomic number (Z^4) and hence in the case of $5d$ elements it is more prominent and an important energy scale to be considered [6,7]. Currently a lot of focus has been on the study of interplay among these two energy scales. Iridate family is being considered as a strong candidate to probe this interplay since the order of magnitude of both electronic correlation and SOC is similar in the case of iridates. On top of that the simultaneous presence of $3d$ and $5d$ elements in the same double perovskite would provide us the ideal opportunity to

study the delicate balance of these two energy scales, resulting in various emergent electronic and magnetic phenomena such as spin-orbital excitons [8,9], SOC controlled ground state [10], absence of long range ordering [11], pressure driven metastability [12], noncollinear multipole moment [13], etc. Recently this has turned into a very active field of research and distinct contributions were made to understand the unusual behavior of SOC driven ground state magnetic properties in the Ir based materials [14–22]. The existence of magnetic ground states that do not simply follow the conventional J_{eff} prescription [23–26] is also being inspected. In spite of enormous efforts, the vast family of double perovskites are not well understood at the material specific level and a gray area exists in understanding the role of SOC in such systems.

Very recently a $3d$-$5d$ compound [(Sr$_{1-x}$Ca$_x$)$_2$FeIrO$_6$] was synthesized and shows very interesting electronic and magnetic properties [27]. It was experimentally found that Sr$_2$FeIrO$_6$ (SFIO) has two magnetic transitions at 45 and 120 K, where the transition at 120 K is reported to be weak. On the other hand, Ca$_2$FeIrO$_6$ (CFIO) has a single transition around 75 K. The magnetic ordering is of antiferromagnetic (AFM) type which was confirmed by the experiments and first principles calculations in the previous report [27]. However, there is no detailed understanding on how this AFM transition is set in these materials with such varied transition temperatures. According to common notion the A site cation should not play any active role in determining the magnetic properties, however, there are few examples [28,29] where the A site cation plays an indirect role in determining the electronic properties. In some cases the nonmagnetic elements can also play a very crucial role in determining the AFM transition temperatures [30]. Therefore, in this context it is very important to understand the magnetic ground state of the (Sr/Ca)$_2$FeIrO$_6$ at the microscopic level in terms of the

*sudipta@iitgoa.ac.in

magnetic exchange interactions. In the previous study [27] it was also shown that these materials belong to the class of SOC driven Mott insulators. However, there is no detailed microscopic analysis of the role played by the SOC in determining the ground state of these materials. Such a study will be indispensable to have a general understanding of SOC driven phases at large.

In this study we perform a comparative investigation of the magnetic ground state in terms of the magnetic exchange interactions of Sr_2FeIrO_6 and Ca_2FeIrO_6. We also discuss the low energy spin model in terms of the real space hopping interactions among the different Fe and Ir sites. We found that the magnetic exchange interactions for the case of CFIO are much stronger than SFIO, where the latter exhibits a substantial frustration effect, which explains the higher AFM transition temperature for the case of CFIO than SFIO, as observed in the experiments. To have a better understanding of the calculated exchange interactions in terms of chemical perspective, we also calculated the corresponding Wannier function of relevant Fe and Ir orbitals. Moreover, we provide a detailed and comprehensive analysis of the nonmonotonic and nontrivial role played by SOC in these two isoelectronic and isovalent compounds, in terms of magnetic moment, magnetization density and calculated SOC matrix elements. Our findings reveal that although these compounds are isoelectronic and isovalent, however, the effective strength of the SOC is very different in these two cases, resulting in varied ground state in these two compounds.

II. CALCULATION METHODOLOGY AND CRYSTAL STRUCTURE

The density-functional theory (DFT) calculations were performed within the plane-wave basis set based on a pseudopotential framework as implemented in the Vienna *abinitio* simulation package (VASP) [31,32]. The generalized gradient approximation (GGA) exchange-correlation functional was employed following the Perdew-Burke-Ernzerhof prescription [33]. The experimentally obtained structures were optimized by relaxing the atomic positions towards equilibrium until the Hellmann-Feynman force becomes less than 0.001 eV/Å, keeping the lattice parameters fixed at their experimentally obtained values. In order to incorporate correlations beyond the scope of GGA, Hubbard U was introduced by performing GGA+U calculations [34,35] with suitable values of U_{eff} (U-J_H) at the Fe (5 eV) and Ir (2 eV) sites. The effect of SOC is introduced as a full-relativistic correction term to the Hamiltonian to understand its interplay with other existing energy scales. The calculations were performed with a plane-wave cutoff of 500 eV and $8 \times 8 \times 6$ k mesh in the Brillouin zone was used for self-consistent calculations. In order to obtain the low energy Hamiltonian, we acquired an *ab-initio* derived maximally localized Wannier function basis [36,37] using downfolding technique. Only the Fe-3d and Ir-t_{2g} orbitals were kept as active degrees of freedom in constructing the low energy Hamiltonian and the rest degrees of freedom were downfolded through the renormalization process, so that the resultant low energy Hamiltonian had the essence of the system as a whole. The constructed Wannier functions are maximally localized in nature, which is ensured
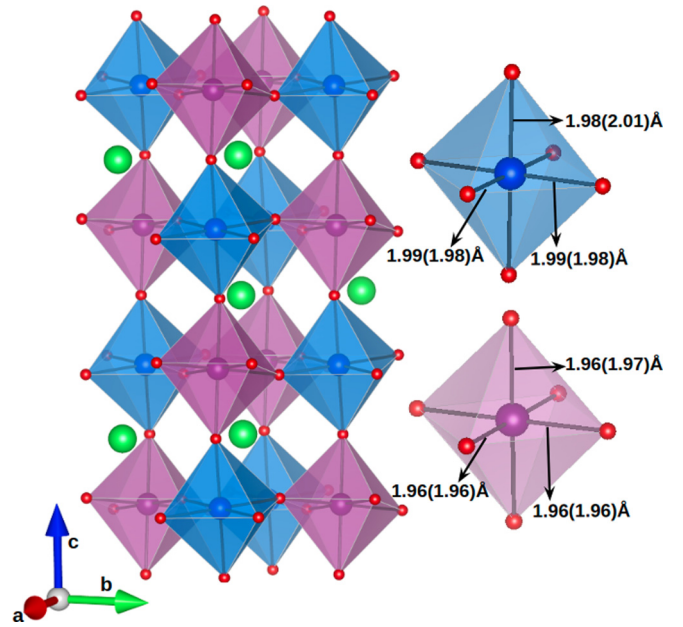

FIG. 1. Crystal structure of $(Sr/Ca)_2FeIrO_6$. Blue and violet polyhedra represent FeO_6 and IrO_6 octahedras, respectively. Green and red spheres represent Sr/Ca and O atoms, respectively. The bond lengths for the FeO_6 and IrO_6 octahedras have been mentioned for SFIO (CFIO).

by setting a low convergence criteria of the gauge-invariant part of the quadratic spread of the Wannier probability distribution to be 10^{-10} Å^2, during the disentanglement of Bloch states. We also obtain a well matched mapping of downfolded Wannier bands on full Bloch states for both SFIO and CFIO (as shown in Fig. S1 of Supplemental Material [38]).

In the literature [26,39–43] it has been reported that Sr_2FeIrO_6 (SFIO) and Ca_2FeIrO_6 (CFIO) stabilizes as a triclinic ($I\bar{1}$) or monoclinic ($P2_1/n$, $I2/m$) space group. However, from the total energy calculations we found that the triclinic space group is energetically lower ($\approx$2 meV/f.u) and henceforth we used the triclinic ($I\bar{1}$) space group for further calculations. The crystal structure is shown in Fig. 1. Both structures consist of corner-sharing alternating octahedras of the Fe and Ir atoms in all three crystallographic directions. Sr/Ca atoms are present in the void spaces in between these octahedras. Both the SFIO and CFIO structures are distorted similar to that of the $GdFeO_3$ type of tilt and rotate structural distortion. FeO_6 and IrO_6 octahedras are distorted in nature and the distortion in terms of bond lengths and bond angles is more pronounced in the case of CFIO as compared to SFIO. In SFIO the $\angle$Fe-O-Ir is 163.6° along c axis and 167.2° in the a-b plane. For CFIO it further deviates to 149.7° along c axis and 155.6° in the a-b plane. The enhanced structural distortion in the case of CFIO, as compared to SFIO, can be explained from the fact that the Ca atom in CFIO has a smaller ionic radius compared to that of the Sr atom in SFIO.

III. ELECTRONIC STRUCTURE

The total energy calculations exhibit that both SFIO and CFIO are in AFM ground state. The orbital projected
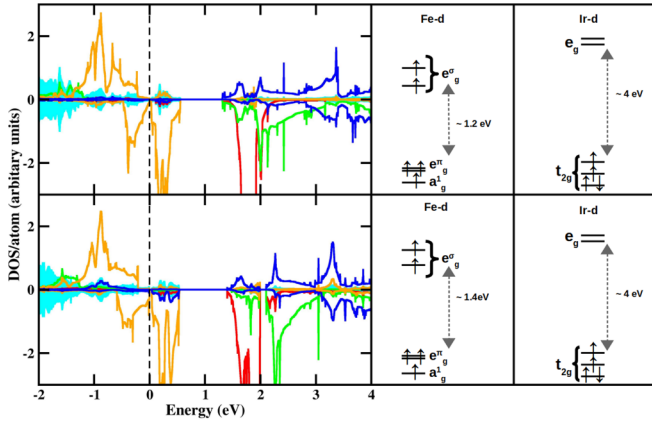
FIG. 2. The calculated GGA+U orbital projected density of states for SFIO (up) and CFIO (down) for the lowest AFM spin configuration is shown in the left side panel. The red, green, orange, blue, and cyan lines represent the Fe-t_{2g}, Fe-e_g, Ir-t_{2g}, Ir-e_g, and O-$2p$ states, respectively. The Fermi energy is set at zero in the energy scale. The right panel shows the corresponding energy level splitting and the occupancy for Fe-3d and Ir-5d states separately. For simplicity, the spins are arranged in ferromagnetic ordering.

density of states for this configuration is shown in Fig. 2. In this AFM ground state configuration, the Fe and Ir spins are antiferromagnetically aligned in the ab plane and ferromagnetically aligned along the crystallographic c direction. Sr (in SFIO) and Ca (in CFIO) density of states lie far away from the Fermi energy level (E_f) which is consistent with them being in Sr^{+2} and Ca^{+2} valence states, respectively. For the AFM configuration, a very small gap is present at the Fermi energy level for both SFIO and CFIO. However, this gap is more pronounced in CFIO as compared to SFIO, due to the enhanced structural distortion in the former. The calculated spin magnetic moments at the Fe sites are 4.09 (4.11) μ_B for the case of SFIO (CFIO) and at the Ir sites are 1.30 (1.28) μ_B for the case of SFIO (CFIO). From Fig. 2 it is clear that the Fe-t_{2g} and Fe-e_g states are completely filled in the majority spin channel (lies around 8 eV below the Fermi level and not shown in this figure) and completely empty in the minority spin channel. The Ir t_{2g} are completely filled in the majority spin channel and partially filled in the minority spin channel, whereas the Ir-e_g states are completely empty in both spin channels. From the combined findings of DOS and calculated magnetic moments we can conclude that Fe is in $+3(3d^5)$ electronic state with a high spin state of $S = \frac{5}{2}$ and Ir is in $+5(5d^4)$ electronic state with a low spin state $S = 1$. The induced magnetic moment at the oxygen sites (~ 0.22 μ_B) is small but non-negligible suggesting there is substantial hybridization among the Fe/Ir-d states with the O-$2p$ states.

Due to the distorted nature of FeO$_6$ and IrO$_6$ octahedras, the degeneracy of t_{2g} and e_g manifolds are lifted as shown in the energy level diagram in the right panel of Fig. 2, without including the spin splitting. The Fe-t_{2g} broadly splits according to the lower lying a_{1g} and upper lying e_g^π symmetry. The energy level splitting of the Fe-d states are alike for both SFIO and CFIO, except that the bandwidth of CFIO (~ 1.4 eV) is slightly larger than SFIO (~ 1.2 eV). The crystal field splitting between t_{2g} and e_g for the Ir-5d states are much larger (~ 4 eV)

compared to the Fe-3d states. Therefore, the Fe-d^5 electrons occupy the five d orbitals in the half-filled configuration resulting in high spin $S = \frac{5}{2}$ state. On the contrary, due to large crystal field splitting between t_{2g} and e_g at the Ir sites, the Ir-d^4 spin prefers to be in the low spin configuration occupying only t_{2g} manifold resulting in $S = 1$ spin state. Additionally, when we include spin-orbit coupling in the calculations, the spin states of the Fe and Ir remains unchanged; $\mu_{Fe}^{spin}(\mu_{Ir}^{spin}) = 4.11(0.62)$ μ_B for SFIO; $\mu_{Fe}^{spin}(\mu_{Ir}^{spin}) = 4.10(0.60)$ μ_B for CFIO, although there are noticeable reductions of the spin moment at the Ir site due to transfer to the orbital part of the magnetic moment. The common perception with iridates is that the electronic structure of iridates should be described in terms J_{eff} prescription. However, in the present case we found that there was substantial magnetic moment at the Ir site, even in the presence of SOC, which discards the $J = 0$ state as expected from the J_{eff} picture [23–26]. This further aids to construct the effective low energy spin model Hamiltonian by taking into account the Fe-d and Ir-t_{2g} states as active degrees of freedom for the systems.

IV. MAGNETIC EXCHANGE INTERACTIONS

There is a dissimilarity in the AFM transition temperatures of SFIO and CFIO as reported from recent experimental study. In this section we provide the microscopic explanation behind this, by calculating magnetic exchange interactions in terms of spin models. The popular method of extracting the underlying model is to fit bulk magnetization data with assumed magnetic models. One significant aspect to be noted here is that this methodology may give rise to nonunique results, due to the fitting parameters. Therefore, electronic structure level understanding is needed for the sake of uniqueness. In simple words, magnetic exchange interaction is the energy difference between the FM and AFM spin configurations. There are various methodologies to compute the magnetic exchange interactions, nevertheless we adopted the methodology based on the total energy calculations for various spin configurations and mapped those energies on the effective Ising model [44,45] of the form of $E^{Tot} = \sum_{ij} J_{ij} S_i^z S_j^z$, where J_{ij} is the magnetic exchange interaction between the ith and jth sites and S_i^z and S_j^z are the effective spins at the corresponding sites. Although there are various drawbacks of this method like choosing the correct spin configurations, exchange path, and exchange-correlation functional, it however gives an estimate of the value and nature of the magnetic exchange interactions reasonable enough to explain the physical picture of the various classes of materials [45–48]. We begun by constructing a $\sqrt{2} \times \sqrt{2} \times 2$ supercell from the parent structure containing eight Fe and eight Ir atoms with a total of 80 atoms in the supercell. We then considered nine independent possible exchange interaction pathways as can be seen in Fig. 3. Out of these nine exchange paths, three are between Fe-Ir, and three each are between different Fe-Fe and Ir-Ir, respectively, as shown in Fig. 3. In our calculations we used $S^z = \frac{5}{2}$ and 1 for Fe and Ir, respectively. Point to be noted here is that the exchange paths are mutually coupled with each other, therefore the obtained algebraic equations for different spin configurations are also mutually coupled and decoupling them
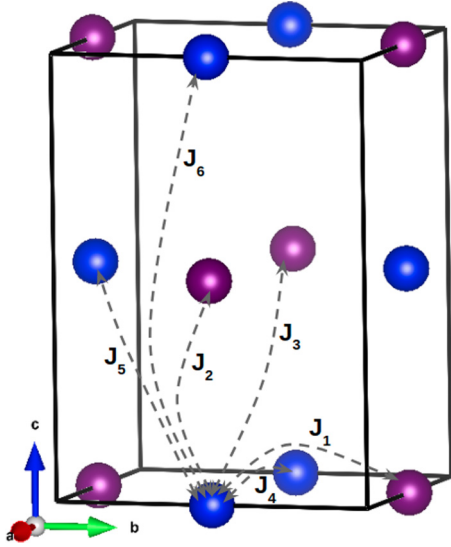
FIG. 3. The possible magnetic exchange interaction pathways are shown in the unit cell of $(Sr/Ca)_2FeIrO_6$. The blue and violet spheres represent Fe and Ir atoms, respectively. J_1-J_3 represent the Fe-Ir interactions and J_4-J_6 depict the Fe-Fe interactions. J_4'-J_6' are the corresponding pathways between the Ir atoms, which has not been drawn in the figure in order to keep it simple. The Sr and O atoms are not shown in the figure for the sake of clarity.

will require more number of the algebraic equations than the number of J's. For our calculation we considered 24 possible spin configurations for both SFIO and CFIO. The total energy expression for the most simplest ferromagnetic configuration can be written as $E^{FM} = -80J_1 - 60J_2 - 60J_3 - 25J_4 - 75J_5 - 50J_6 - 16J_4' - 48J_5' - 32J_6'$.

In a similar manner we constructed the algebraic equations for other spin configurations. These equations were solved simultaneously to obtain the values of exchange interaction J's. The J values thus calculated using $U_{eff}^{Fe} = 5$ eV and $U_{eff}^{Ir} = 2$ eV for both SFIO and CFIO are shown in Table I. We found that the exchange interaction strengths for SFIO are smaller compared to that of the corresponding J's of CFIO. This is in close agreement with the fact that the transition

TABLE I. The GGA+U ($U_{eff}^{Fe} = 5$ eV and $U_{eff}^{Ir} = 2$ eV) calculated magnetic exchange interactions for different paths for SFIO and CFIO, as shown in Fig. 3. The values listed in the table are calculated from the $\sqrt{2} \times \sqrt{2} \times 2$ supercell as mentioned in the main text.

| J's | Interaction paths | SFIO | | CFIO | |
		J (meV)	Type	J (meV)	Type
J_1	Fe-Ir in-plane	15.6	FM	23.2	AFM
J_2	Fe-Ir out-of-plane	6.5	AFM	16.9	FM
J_3	Fe-Ir out-of-plane	7.9	AFM	15.6	FM
J_4	Fe-Fe in-plane	24	AFM	30.7	AFM
J_5	Fe-Fe out-of-plane	7.4	FM	55.9	AFM
J_6	Fe-Fe out-of-plane	10.4	AFM	10.5	AFM
J_4'	Ir-Ir in-plane	2.1	FM	5.7	FM
J_5'	Ir-Ir out-of-plane	71.4	AFM	75.7	AFM
J_6'	Ir-Ir out-of-plane	4.1	FM	11.9	FM

temperature for CFIO (75 K) is found to be greater than that of SFIO (45 K). We calculated three different types of exchange interactions; intersublattice (J_1, J_2 and J_3) between Fe and Ir, intrasublattices between different Fe (J_4, J_5, and J_6) and Ir (J_4', J_5', and J_6') sites, respectively. From Table I we can see that for SFIO the intersublattice Fe-O-Ir in-plane FM superexchange interaction (i.e., J_1) is stronger than the other Fe-Ir out-of-plane AFM superexchange interactions (i.e., J_2 and J_3). For the case of CFIO, we also observed the same trend, i.e., the J_1 is stronger than the J_2 and J_3, however, nearest neighbor Fe-O-Ir (J_1) superexchange is AFM type, whereas the out-of-plane exchange interactions (i.e., J_2 and J_3) are of the FM type and the strengths are stronger in the case of CFIO than the SFIO. We also found that the Fe and Ir intrasublattice interactions are stronger than the Fe-Ir intersublattice interactions. For example, the in-plane Fe-O-Ir-O-Fe (J_4) and out-of-plane Ir-O-Fe-O-Ir (J_5') super-superexchange interactions are the strongest intrasublattice interactions for SFIO and out-of-plane Fe-O-Ir-O-Fe (J_5) and Ir-O-Fe-O-Ir (J_5') super-superexchange interactions are the strongest intrasublattice interactions for CFIO. All these superexchange interactions are of the AFM type in nature. From this we can infer that the intersublattice (Fe-Ir) orders in a different manner as compared to the intrasublattices (Fe-Fe or Ir-Ir). An interesting fact is that for both SFIO and CFIO the in-plane Ir-Ir FM superexchange interaction (J_4') is much smaller than that of the out-of-plane AFM interaction (J_5'). For the in-plane FM interaction the electrons need to hop from the Ir-t_{2g} subband to the Ir-e_g subband, which are separated by the large crystal field splitting of around 4 eV and therefore is less probable. On the contrary, the electron hopping within the Ir-t_{2g} manifold is more probable, which leads to the AFM interactions along the out-of plane direction. Point to be noted is that the most dominant exchange interaction is the Ir-O-Fe-O-Ir out-of-plane interaction (J_5') for both SFIO and CFIO, due to the fact that 5d-Ir orbitals are much more extended than 3d-Fe orbitals. We also crosschecked the calculated J values for both SFIO and CFIO with other combinations of the U values at both Fe and Ir sites as shown in Tables S2 and S3 in Supplemental Material [38]. We found that although with the variation of U, the obtained J values varies as expected, however the type of the interactions and the major trend of J's remain unchanged. Since, for these two materials, SOC is a crucial energy scale, it is indeed essential to check the exchange interactions in the presence of SOC. Consequently we calculated the magnetic exchange interactions, including SOC in the total energy calculations (GGA+U+SOC), as shown in the Supplemental Material Table S1 [38]. In spite of the fact that there is a change in the absolute values as compared to the GGA+U results, there is no alteration in the basic trend of J values with the inclusion of the SOC.

In order to have a comprehensive picture of exchange interactions, we calculated the intraplane and interplane hopping matrix corresponding to the exchange interactions paths for SFIO shown in Table II. The Fe-Ir, Fe-Fe, and Ir-Ir hopping matrices are 3×5, 5×5, and 3×3 matrices, respectively, as all five d orbitals for Fe and only three t_{2g} orbitals for Ir are active degrees of freedom. Comparing the dominant interactions for the Fe-Ir sublattice, we find that the in-plane

TABLE II. List of hopping interactions between Fe-Ir, Fe-Fe, and Ir-Ir atoms in SFIO. Fe-Ir interactions are defined among the five Fe-d and three Ir-t_{2g}. Fe-Fe interactions are defined among the five Fe-d orbitals and Ir-Ir interactions are defined among the three Ir-t_{2g} orbitals.

Interacting sites	In-plane matrix					Out-of-plane matrix				
	d_{xy}	d_{yz}	$d_{3z^2-r^2}$	d_{xz}	$d_{x^2-y^2}$	d_{xy}	d_{yz}	$d_{3z^2-r^2}$	d_{xz}	$d_{x^2-y^2}$
Fe-Ir =										
d_{xy}	0.28	0.03	0.02	0.02	0.10	0.07	−0.00	−0.04	−0.01	0.08
d_{yz}	−0.02	−0.11	0.01	−0.08	0.03	−0.00	−0.11	0.00	0.11	0.00
d_{xz}	−0.02	−0.10	−0.00	−0.10	0.00	−0.02	0.06	0.01	−0.08	0.01

Fe-Fe =	d_{xy}	d_{yz}	$d_{3z^2-r^2}$	d_{xz}	$d_{x^2-y^2}$	d_{xy}	d_{yz}	$d_{3z^2-r^2}$	d_{xz}	$d_{x^2-y^2}$
d_{xy}	−0.17	0.01	0.01	0.01	−0.00	−0.15	0.00	0.00	0.01	0.00
d_{yz}	0.01	−0.00	0.00	0.00	0.01	0.00	−0.01	0.00	0.00	0.00
$d_{3z^2-r^2}$	0.01	0.00	−0.03	−0.01	0.00	0.00	0.00	−0.05	−0.01	−0.01
d_{xz}	0.01	0.00	−0.01	−0.01	0.00	0.01	0.00	−0.01	0.00	−0.00
$d_{x^2-y^2}$	−0.00	0.01	0.00	0.00	0.03	0.00	0.00	−0.01	−0.00	0.03

Ir-Ir =	d_{xy}	d_{yz}	d_{xz}	d_{xy}	d_{yz}	d_{xz}
d_{xy}	−0.11	−0.01	−0.01	−0.21	−0.01	−0.01
d_{yz}	−0.01	0.07	0.00	−0.01	−0.02	−0.00
d_{xz}	−0.01	0.00	−0.00	−0.01	−0.00	0.02

interaction is much stronger than the out-of-plane interaction. A similar kind of trend can also be visualized in the case of the Fe-Fe sublattice. However, in the case of the Ir-Ir sublattice, the trend is opposite, i.e., the out-of-plane interactions are much stronger than in-plane interactions. A very important realization is that the electronic hopping integrals are in complete agreement with the calculated values of J from the total energy calculations mentioned in Table I.

The above trend of exchange interactions can be additionally understood via the chemical perspective by looking at the corresponding Wannier functions, constructed using five Fe-d orbitals and three Ir-t_{2g} orbitals, as shown in Figs. 4 and 5 for SFIO and CFIO, respectively. The rationality behind choosing these orbitals and integrating out the Sr/Ca, O, and Ir-e_g orbitals is that they are the active orbitals near the Fermi energy and are responsible for magnetism in these materials. Although in general Wannier functions are not uniquely defined due to their complexity, and their nature de-

pends on various technical details; however, the construction of the maximally localized Wannier orbitals provides a way to uniquely define Wannier orbitals that incorporates effects of ligand orbitals such as O-$2p$. These maximally localized Wannier functions are broadly used to understand chemical nature and interactions and are able to satisfactorily provide a chemical picture of the effective superexchange interaction paths for a wide range of complex materials [30,46,49–57]. In the present case, to describe the superexchange interactions between two magnetic sites, the uniquely defined maximally localized Wannier orbitals are constructed in the basis set of Fe-$3d$ and Ir-t_{2g} orbitals, where the effect of the O-$2p$ ligands in the superexchange interactions are taken care through the renormalization effect.

The central part of the maximally localized Wannier functions are shaped according to the plotted Fe-$3d$ or Ir-$5d$ orbital characters, whereas the tails situated at other atoms show the effect of the orbitals which were renormalized. The weight of
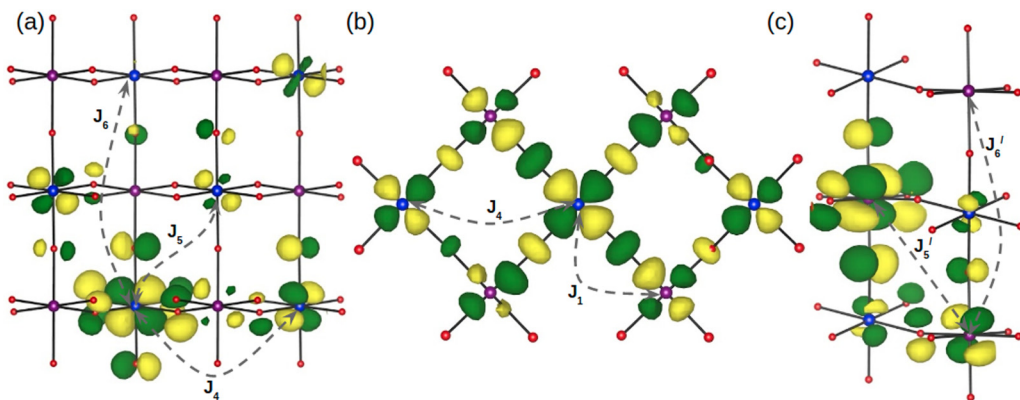

FIG. 4. SFIO Wannier functions of (a) Fe-$3d_{yz}$ (b) Fe-$3d_{x^2-y^2}$, and (c) Ir-$5d_{xz}$ centered at Fe and Ir sites, respectively. The exchange interactions J_4-J_6, J_1-J_4, and J_5'-J_6' are shown in (a)–(c) respectively. Yellow and green color lobes represent isosurfaces with positive and negative signs. Color convention of the atoms is the same as that of Figs. 1 and 3.

FIG. 5. CFIO Wannier functions of (a) Fe-$3d_{yz}$, (b) Fe-$3d_{x^2-y^2}$, and (c) Ir-$5d_{xz}$ centered at Fe and Ir sites, respectively. The exchange interactions J_4-J_6, J_1-J_4, and J_5'-J_6' are shown in (a)–(c), respectively. Yellow and green color lobes represent isosurfaces with positive and negative signs. Color convention of the atoms is the same as that of Figs. 1 and 3.
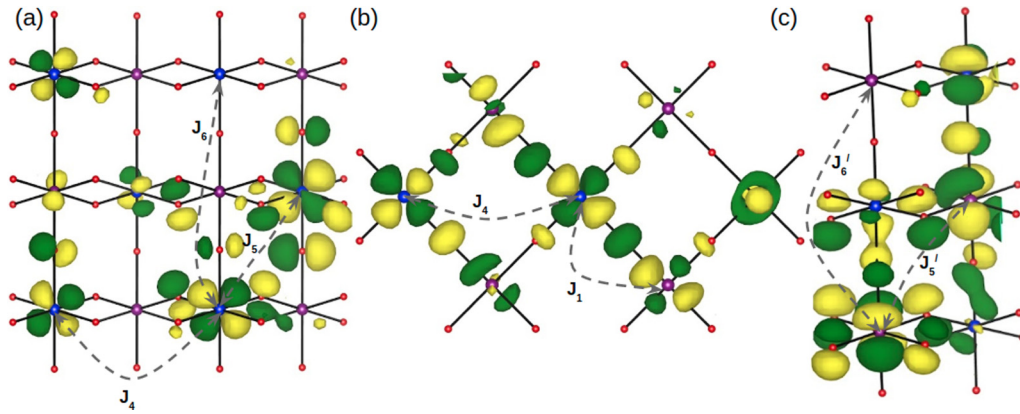
the tails at neighboring atoms dictates the strength of the inter-action between the connected atomic sites. Figure 4(a) shows the central part is of the Fe-$3d_{yz}$ orbital character and the tails situated at different Fe and Ir sites indicate the strength of the interaction with the central Fe site. It shows that for the SFIO Fe-O-Ir-O-Fe in-plane AFM interactions (J_4) are much stronger than Fe-O-Ir-O-Fe out-of-plane FM interactions (J_5), as shown in Fig. 4(a), whereas for CFIO, J_5 is stronger than the J_4 as indicated by the weightage of the tail part connecting to the respective Fe sites in Fig. 5(a). The strong in-plane Fe-Fe AFM superexchange interactions are expected due to the half-filled d orbitals. Moving towards the intersublattice (Fe and Ir) interaction, the nearest neighbor interaction through Fe-O-Ir superexchange path (J_1) is the strongest for both SFIO and CFIO among other intersublattice interactions (i.e., J_2 and J_3). Point to be noted is that, from Figs. 4(b) and 5(b) we can see that the Fe-O-Ir (J_1) and Fe-O-Ir-O-Fe interaction (J_4) are almost of the same order of magnitude as reflected by the similar weightage of the tail. An interesting observation is that in both SFIO and CFIO the Ir-O-Fe-O-Ir out-of plane interaction (J_5') is the strongest among all other interactions, which can be understood from the extended nature of the $5d$ orbitals of the Ir and that can be verified from Figs. 4(c) and 5(c).

The comparative trend of the magnetic ground state of SFIO and CFIO can be understood from the qualitative trend of the evaluated magnetic exchange interactions. Using the spin configuration shown in Fig. 6, the competition among the different exchange interactions can be understood. For the case of CFIO, in these given spin configurations the strongest intrasublattice interactions, i.e., AFM J_5 and J_5' superexchange interactions between Fe-O-Ir-O-Fe and Ir-O-Fe-O-Ir sites, respectively, can be satisfied simultaneously. Moreover, the intersublattice interactions, i.e., AFM J_1 and FM J_2 superexchange between Fe-O-Ir, can also be satisfied. The Ir-Ir long range weak FM J_6' interaction also gets satisfied, however, next-nearest neighbor Fe-Fe AFM superexchange interaction along J_6 is not satisfied due the competition with the strong FM J_2 interaction. Since J_2 is stronger then J_6, in this competition, J_2 wins over J_6, establishing the given spin configuration. However, for the case of SFIO, most of the exchange interactions tabulated in Table I cannot be satisfied simultaneously,

except for the strongest Ir-O-Fe-O-Ir AFM superexchange interaction J_5' due to strong competition. All these contradictory exchange interactions introduce vigorous competition among the different FM and AFM exchange interactions of SFIO, which leads to strong frustration in the system, which
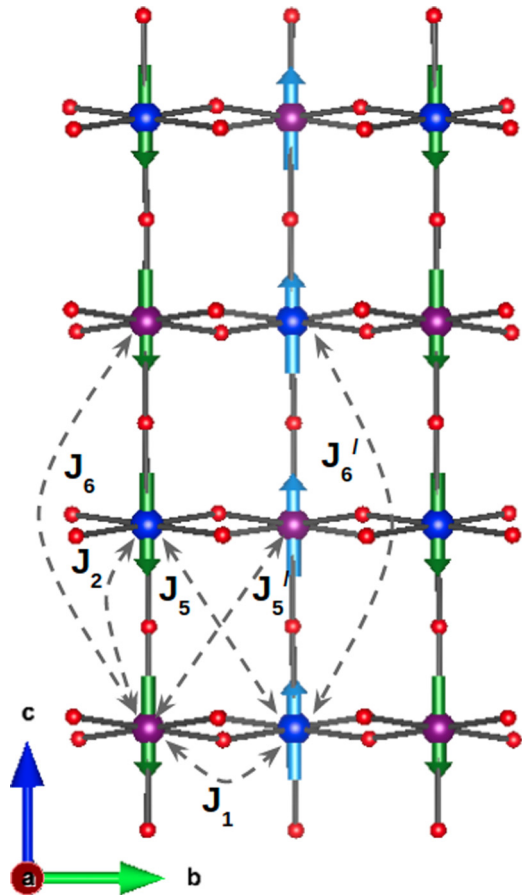

FIG. 6. The exchange interactions of hopping paths J_1, J_2, J_5, J_5', J_6, and J_6' presented in a schematic way, in the lowest AFM spin configuration. The same spin configuration was employed to reproduce the DOS in Fig. 2. The atoms color convention is the same as that of Figs. 1 and 3.
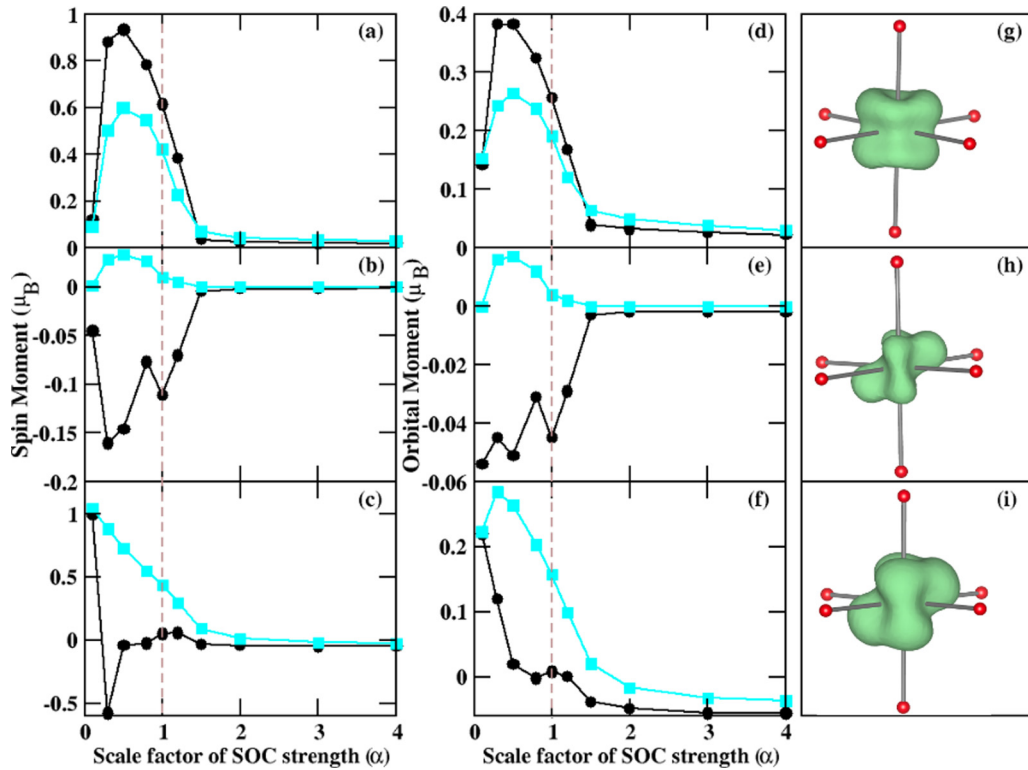
FIG. 7. The variation of the magnetic moment at the Ir site with respect to the change in SOC strength scaling factor (α). (a)–(c) The spin magnetic moment along m_x, m_y, and m_z, respectively. (d)–(f) The orbital magnetic moment along o_x, o_y, and o_z, respectively. The circle (dark line) and square (light line) represent the SFIO and CFIO, respectively. The parent strength ($\alpha = 1$) of the SOC has been marked by a vertical dotted line. (g) The magnetization density (m_x) at the Ir site for SFIO, (h) the magnetization density (m_z) at the Ir site for CFIO, at parent SOC strength ($\alpha = 1$), and (i) the magnetization density (m_z) at the Ir site for SFIO, at $\alpha = 0.1$.

is clearly more dominating than the CFIO compound, and is also consistent with the experimental observations [27]. To overcome the strong frustration, SFIO exhibits long range AFM ordering at much lower temperature (45 K) than CFIO (75 K), which has been observed in the experiments. An important point that needs to be highlighted here is that the dominant exchange interactions of SFIO are quite compatible with the experimental measurements obtained through neutron diffraction. For example, the nature of the strong intrasublattices interactions (AFM J_4, FM J_5, AFM J_6, and AFM J_5') are consistent with each other.

V. ROLE OF THE SPIN-ORBIT COUPLING

Next we would like to investigate the effect of SOC on the emerging electronic structure of both SFIO and CFIO. Since in both SFIO and CFIO Ir is in the same electronic configuration, ideally the effect of SOC should be the same, as SOC is an intrinsic atomic property. However, the effect of SOC is very different on SFIO as compared to CFIO which can be visualized in the magnetization density plots with GGA+U+SOC in Figs. 7(g) and 7(h). One of the major differences that one can see from Fig. 7 is that the Ir magnetization density is majorly along the m_x component for SFIO and in the m_x-m_z plane for CFIO. The other major difference is in the shape of Ir magnetization density between SFIO and CFIO. For the case of SFIO the magnetization density shapes [Fig. 7(g)] are very similar, to what one can expect for

the d^4 electronic configuration at the t_{2g} manifold. However, in the case of CFIO, the shape of the magnetization density [Fig. 7(h)] is more distorted than what one can expect from the d^4 electronic configuration at the t_{2g} manifold. The distorted shape is due to the competition between the strength of SOC and the crystal structural distortion. For the case of CFIO the structural distortion is more prominent than the SFIO, which dilutes the effective strength of the SOC in the case of CFIO as compared to SFIO.

To understand the different role played by SOC in more detail, we performed a comparative investigation of the electronic structures by tuning the strength of SOC for both SFIO and CFIO in our calculations. In our attempt to do so, we varied the SOC strength scale factor (α) from 0.1 to 4.0. By changing the α we could tune the strength of the SOC from 0.1 times to 4 times of the original SOC strength. We cross-checked our methodology by matching the magnetization density plot of GGA+U+SOC at $\alpha = 0.1$ with the GGA+U magnetization density plot and found them to be consistent [23]. As expected, we did not find any major changes in the magnetic moment at the Fe site for both SFIO and CFIO, with the variation in SOC strength scale factor α. However, a nonmonotonic variation of the spin and orbital magnetic moments at Ir site was seen, which is quite similar for both SFIO and CFIO, shown in Figs. 7(a)–7(f). With $\alpha = 1$, i.e., the parent strength of the SOC, the Ir spin moment is completely aligned in the m_x component for SFIO, while Ir spin moments are in the m_x-m_z component for CFIO. When we decreased the

value of α from 1, m_x component initially increased and then decreased close to zero, whereas the m_z component increased close to the saturation value, as shown in Figs. 7(a)–7(c). A very interesting variation trend was found for the case of the orbital moment as a function of α, as shown in Figs. 7(d)–7(f). For SFIO, the x component of the orbital moment (o_x) is dominating, whereas in the case of the CFIO the orbital moment is distributed between the o_x and o_z components for $\alpha = 1$. As we reduced the scale factor of SOC strength of α, the orbital moment initially increased and then decreased for both SFIO and CFIO. However, one fascinating observation is that the variation of the z component of spin and orbital moments behave very differently for the case of SFIO, as compared to CFIO. Moreover, their magnitudes are also quite different. Remarkably, when we increased the α from 1, we found that the moment decreased close to zero, which indicated that with the increase of strength of SOC the energy gap within the t_{2g} manifold increased, pushing the d^4 electronic configuration to the low spin state. Point to be noted is that the peak values of the magnetic moments for the case of SFIO is much higher than that of CFIO.

The effect of the SOC is more prominent on the Ir states compared to the Fe states. We calculated the magnetization or spin density at the Ir sites by changing the SOC strength (α). The investigation of the shape of the outermost orbitals (in this case the spin density) carries very important information about the effect of the SOC on the orbitals as it modifies the shape of the orbitals after combining with the spin degrees of freedom. In literature, specifically for the case of iridates, the modification in the shape of the orbitals has been discussed to understand the effect of the SOC [7,23,58,59]. In the current scenario the magnetization density, or more explicitly the spin density, plays an equivalent role. In the present case, both SFIO and CFIO have the same spin and charge state, so it is interesting to compare the magnetization or spin density, where the other factors such as SOC modifies the shape of the complex orbitals. The magnetization or spin density gives us the information of the outermost partially filled orbitals, which is responsible for magnetism. In the presence of SOC, the orbital and spin degrees of freedom are coupled, therefore the shape will no longer be similar to that of the only orbital characteristic and carries the information about the effect of SOC.

Comparing the shape of the magnetization or spin densities [Figs. 7(g)–7(i)], it is very clear that the shape of the Ir magnetization density of SFIO has become more distorted [Fig. 7(i)] with reduced SOC strength scale factor ($\alpha = 0.1$) compared to the magnetization density [Fig. 7(g)] with parent SOC strength ($\alpha = 1$), due the enhanced competition between the SOC and the structural distortion, as the parent SOC strength has weakened at $\alpha = 0.1$. A more engrossing fact is that if we compare Fig. 7(h) with Fig. 7(i), i.e., CFIO magnetization density with $\alpha = 1$ and SFIO magnetization density with $\alpha = 0.1$, the shape looks very similar to each other, except size of the isosurface, which is due to the difference in spin moments. This exercise indicated that the effective strength of the SOC is larger in the case of SFIO compared to that of CFIO. A possible explanation of this could be the fact that the larger structural distortion in CFIO competes with SOC to decrease its relative strength. In the present case,

due to competition with the structural distortion, the relative strength of the SOC gets modified differently in the case of SFIO and CFIO. As we know that the SOC is an intrinsic property of the elements, which is proportional to the Z^4 of the element. SFIO and CFIO are isoelectronic and isovalent materials, where we can expect the behavior/effect of the SOC should be the same. Nonetheless, due to the competition with other energy scales, the SOC driven shape of the spin density is more distorted in the case of CFIO than SFIO. Now when we reduce the α, which is equivalent to the reduction of the relative strength of SOC for SFIO, the shape of the spin density of SFIO replicates that of CFIO with parent SOC strength.

To further analyze the discrete effect of SOC on SFIO and CFIO, we computed the eigenvalues through the diagonalizing the spin-averaged SOC matrix [60] for the Ir-d states, at two different strengths of SOC, say parent strength, i.e., ($\alpha = 1$) in (1) and (2) and double of the parent strength, i.e., ($\alpha = 2$) in (3) and (4) for SFIO and CFIO, respectively,

$$H_{\text{SOC}}^{\text{SFIO}}(\alpha = 1) = (-0.264, 0.171, 0.082, 0.062, -0.051), \tag{1}$$

$$H_{\text{SOC}}^{\text{CFIO}}(\alpha = 1) = (-0.243, 0.166, 0.084, -0.076, 0.069), \tag{2}$$

$$H_{\text{SOC}}^{\text{SFIO}}(\alpha = 2) = (-0.776, 0.488, 0.308, -0.253, 0.233), \tag{3}$$

$$H_{\text{SOC}}^{\text{CFIO}}(\alpha = 2) = (-0.768, 0.511, 0.337, -0.286, 0.206). \tag{4}$$

Although in both cases, Ir is in the same nominal valance and charge states, we obtain a different set of eigenvalues for SFIO and CFIO. Moreover, the ordering of the sign of the eigenvalues differ for the case of the $H_{\text{SOC}}^{\text{SFIO}}(\alpha = 1)$ and $H_{\text{SOC}}^{\text{CFIO}}(\alpha = 1)$, which indicates that SOC affects SFIO and CFIO in nonidentical fashion. When we compare the eigenvalues at double of the parent SOC strength, i.e., with $\alpha = 2$, we find that the ordering of the sign of the eigenvalues of SFIO is similar to that of the CFIO. With twice the SOC strength, the orbitals of SFIO behave equivalently to those of CFIO. This exercise demonstrates that the effect of SOC on the specific orbitals vary in the case of SFIO and CFIO. At the same time, it implies that the role played by SOC, in competition to other energy scales, is not equivalent in both of these materials due to the delicate balance in the energy scales.

VI. CONCLUSION

In conclusion, we studied the ground state magnetic properties of Sr_2FeIrO_6 and Ca_2FeIrO_6 and the effect of SOC using $ab - initio$ first principles calculations. From the calculated magnetic exchange interaction and the Wannier functions we addressed the difference in the AFM transition temperature observed for SFIO and CFIO in the experiments. We found that the strength of the magnetic exchange interactions are stronger in CFIO than SFIO, with a dominant signature of frustration in SFIO. This explains the lower transition temperature in SFIO than CFIO. We also found that in both compounds, Ir-Ir intrasublattice exchange interactions

are dominant over others, which has been visualized from the chemical viewpoint through the Wannier function plot. To understand the role played by SOC in these cases, we calculated the variation of magnetic moments, SOC Hamiltonian matrix elements, and magnetization densities as a function of the strength of SOC. We found very interesting nonmonotonic variation both in spin and orbital magnetic moments for SFIO and CFIO. Our analysis reveals that in spite of the SFIO and CFIO being isoelectronic and isovalent, the effect of SOC is not the same in these two compounds. Due to the competition with the structural distortion, the effective strength of SOC is reduced in CFIO compared to that of SFIO. Our investigations reveal the nontrivial role of SOC in estab-lishing the ground state magnetic properties of the Ir based double-perovskite compounds and open up the avenue to design the quantum phases by tuning the SOC and will be helpful in understanding a wide range of $5d$ based quantum materials in general.

[1] K. I. Kobayashi, T. Kimura, H. Sawada, K. Terakura, and Y. Tokura, Nature (London) **395**, 677 (1998).

[2] H. Kato, T. Okuda, Y. Okimoto, and Y. Tomioka, Appl. Phys. Lett. **81**, 328 (2002).

[3] J. B. Philipp, P. Majewski, L. Alff, A. Erb, R. Gross, T. Graf, M. S. Brandt, J. Simon, T. Walther, W. Mader, D. Topwal, and D. D. Sarma, Phys. Rev. B **68**, 144431 (2003).

[4] H. L. Feng, S. Calder, M. P. Ghimire, Y. H. Yuan, Y. Shirako, Y. Tsujimoto, Y. Matsushita, Z. Hu, C. Y. Kuo, L. H. Tjeng, T. W. Pi, Y. L. Soo, J. He, M. Tanaka, Y. Katsuya, M. Richter, and K. Yamaura, Phys. Rev. B **94**, 235158 (2016).

[5] B. Singh, M. Vogl, S. Wurmehl, S. Aswartham, B. Büchner, and P. Kumar, Phys. Rev. Research **2**, 013040 (2020).

[6] B. J. Kim, H. Jin, S. J. Moon, J. Y. Kim, B.-G. Park, C. S. Leem, J. Yu, T. W. Noh, C. Kim, S. J. Oh, J. H. Park, V. Durairaj, G. Cao, and E. Rotenberg, Phys. Rev. Lett. **101**, 076402 (2008).

[7] B. J. Kim, H. Ohsumi, T. Komesu, S. Sakai, T. Morita, H. Takagi, and T. Arima, Science **323**, 1329 (2009).

[8] B. H. Kim, D. V. Efremov, and J. van den Brink, Phys. Rev. Materials **3**, 014414 (2019).

[9] M. Kusch, V. M. Katukuri, N. A. Bogdanov, B. Büchner, T. Dey, D. V. Efremov, J. E. Hamann-Borrero, B. H. Kim, M. Krisch, A. Maljuk, M. M. Sala, S. Wurmehl, G. Aslan-Cansever, M. Sturza, L. Hozoi, J. van den Brink, and J. Geck, Phys. Rev. B **97**, 064421 (2018).

[10] A. E. Taylor, R. Morrow, R. S. Fishman, S. Calder, A. I. Kolesnikov, M. D. Lumsden, P. M. Woodward, and A. D. Christianson, Phys. Rev. B **93**, 220408(R) (2016).

[11] H. Schnait, D. Bauernfeind, T. Saha-Dasgupta, and M. Aichhorn, Phys. Rev. B **106**, 035132 (2022).

[12] M. A. Laguna-Marco, E. Arias-Egido, V. Cuartero, I. Herrero-Albillos, P. Kayser, J. A. Alonso, G. Fabbris, D. Haskel, and T. Irifune, Phys. Rev. B **105**, 064421 (2022).

[13] S. W. Lovesey, D. D. Khalyavin, G. van der Laan, and G. J. Nilsen, Phys. Rev. B **103**, 104429 (2021).

[14] P. Kayser, B. J. Kennedy, B. Ranjbar, J. A. Kimpton, and M. Avdeev, Inorg. Chem. **56**, 2204 (2017).

[15] M. Ye, H.-S. Kim, J.-W. Kim, C.-J. Won, K. Haule, D. Vanderbilt, S.-W. Cheong, and G. Blumberg, Phys. Rev. B **98**, 201105(R) (2018).

[16] J. Dai, Y. Yin, X. Wang, X. Shen, Z. Liu, X. Ye, J. Cheng, C. Jin, G. Zhou, Z. Hu, S. Weng, X. Wan, and Y. Long, Phys. Rev. B **97**, 085103 (2018).

[17] P. K. Das, J. Slawiska, I. Vobornik, J. Fujii, A. Regoutz, J. M. Kahk, D. O. Scanlon, B. J. Morgan, C. McGuinness, E. Plekhanov, D. DiSante, Y.-S. Huang, R.-S. Chen, G. Rossi, S. Picozzi, W. R. Branford, G. Panaccione, and D. J. Payn, Phys. Rev. Materials **2**, 065001 (2018).

[18] S. Agrestini, K. Chen, C.-Y. Kuo, L. Zhao, H.-J. Lin, C.-T. Chen, A. Rogalev, P. Ohresser, T.-S. Chan, S.-C. Weng, G. Auffermann, A. Volzke, A. C. Komarek, K. Yamaura, M. W. Haverkort, Z. Hu, and L. H. Tjeng, Phys. Rev. B **100**, 014443 (2019).

[19] R. Morrow, A. E. Taylor, D. J. Singh, J. Xiong, S. Rodan, A. U. B. Wolter, S. Wurmehl, B. Büchner, M. B. Stone, A. I. Kolesnikov, A. A. Aczel, A. D. Christianson, and P. M. Woodward, Sci. Rep. **6**, 32462 (2016).

[20] D. Reig-i-Plessis, T. A. Johnson, K. Lu, Q. Chen, J. P. C. Ruff, M. H. Upton, T. J. Williams, S. Calder, H. D. Zhou, J. P. Clancy, A. A. Aczel, and G. J. MacDougall, Phys. Rev. Materials **4**, 124407 (2020).

[21] H. Hanate, T. Hasegawa, S. Hayami, S. Tsutsui, S. Kawano, and K. Matsuhira, J. Phys. Soc. Jpn. **90**, 063702 (2021).

[22] S.-H. Jang and Y. Motome, Phys. Rev. Materials **5**, 104409 (2021).

[23] S. Kanungo, K. Mogare, B. Yan, M. Reehuis, A. Hoser, C. Felser, and M. Jansen, Phys. Rev. B **93**, 245148 (2016).

[24] S. Bhowal, S. Baidya, I. Dasgupta, and T. Saha-Dasgupta, Phys. Rev. B **92**, 121113(R) (2015).

[25] M. M. Sala, K. Ohgushi, A. Al-Zein, Y. Hirata, G. Monaco, and M. Krisch, Phys. Rev. Lett. **112**, 176402 (2014).

[26] J. E. Page, C. V. Topping, A. Scrimshire, P. A. Bingham, S. J. Blundell, and M. A. Hayward, Inorg. Chem. **57**, 10303 (2018).

[27] K. C. Kharkwal, R. Roy, H. Kumar, A. K. Bera, S. M. Yusuf, A. K. Shukla, K. Kumar, S. Kanungo, and A. K. Pramanik, Phys. Rev. B **102**, 174401 (2020).

[28] D. Lahiri, T. Shibata, S. Chattopadhyay, S. Kanungo, T. Saha-Dasgupta, R. S. Singh, S. M. Sharma, and K. Maiti, Phys. Rev. B **82**, 094440 (2010).

[29] S. Kanungo, R. Datta, S. K. Panda, and T. Saha-Dasgupta, J. Phys.: Condens. Matter **25**, 505503 (2013).

[30] S. Kanungo, B. Yan, C. Felser, and M. Jansen, Phys. Rev. B **93**, 161116(R) (2016).

[31] G. Kresse and J. Hafner, Phys. Rev. B **47**, 558(R) (1993).

[32] G. Kresse and J. Furthmüller, Phys. Rev. B **54**, 11169 (1996).

[33] J. P. Perdew, K. Burke, and M. Ernzerhof, Phys. Rev. Lett. **77**, 3865 (1996)

[34] V. I. Anisimov, I. V. Solovyev, M. A. Korotin, M. T. Czyzyk, and G. A. Sawatzky, Phys. Rev. B **48**, 16929 (1993).

[35] S. L. Dudarev, G. A. Botton, S. Y. Savrasov, C. J. Humphreys, and A. P. Sutton, Phys. Rev. B **57**, 1505 (1998).

[36] A. A. Mostofi, J. R. Yates, Y.-S. Lee, I. Souza, D. Vanderbilt, and N. Marzari, Comput. Phys. Commun. **178**, 685 (2008).

[37] G. Pizzi, V. Vitale, R. Arita, S. Blügel, F. Freimuth, G. Granton, M. Gibertini, D. Gresch, C. Johnson, T. Koretsune, J. Ibaez-Azpiroz, H. Lee, J. Lihm, D. Marchand, A. Marrazzo, Y. Mokrousov, J. I. Mustafa, Y. Nohara, Y. Nomura, L. Paulatto, S. Ponc, T. Ponweiser, J. Qiao, F. Thle, S. S Tsirkin, M. Wierzbowska, N. Marzari, D. Vanderbilt *et al.*, J. Phys.: Condens. Matter **32**, 165902 (2020).

[38] See Supplemental Material at http://link.aps.org/supplemental/10.1103/PhysRevB.106.125113 for the downfolded Wannier band mapped on the full DFT band for SFIO and CFIO; the calculated value of magnetic exchange interactions for SFIO and CFIO with SOC interactions; the calculated value of magnetic exchange interactions for SFIO with the variation in U_{eff} at Fe and Ir sites; and the calculated value of magnetic exchange interactions for CFIO with the variation in U_{eff} at Fe and Ir sites.

[39] K. C. Kharkwal and A. K. Pramanik, J. Phys.: Condens. Matter **29**, 495801 (2017).

[40] P. D. Battle, G. R. Blake, T. C. Gibb, and J. F. Vente, J. Solid State Chem. **145**, 541 (1999).

[41] I. Qasim, P. E. R. Blanchard, S. Liu, C. Tang, B. J. Kennedy, M. Avdeev, and J. A. Kimpton, J. Solid State Chem. **206**, 242 (2013).

[42] L. Bufaiçal, L. T. Coutrim, T. O. Santos, H. Terashita, C. B. R. Jesus, P. G. Pagliuso, and E. M. Bittar, Mater. Chem. Phys. **182**, 459 (2016).

[43] L. Bufaiçal, C. Adriano, R. Lora-Serrano, J. G. S. Duque, L. Mendona-Ferreira, C. Rojas-Ayala, E. Baggio-Saitovitch, E. M. Bittar, and P. G. Pagliuso, J. Solid State Chem. **212**, 23 (2014).

[44] C. S. Hellberg, W. E. Pickett, L. L. Boyer, H. T. Stokes, and M. J. Mehl, J. Phys. Soc. Jpn. **68**, 3489 (1999).

[45] V. V. Mazurenko, F. Mila, and V. I. Anisimov, Phys. Rev. B **73**, 014418 (2006).

[46] S. Kanungo, B. Yan, M. Jansen, and C. Felser, Phys. Rev. B **89**, 214414 (2014).

[47] J. Sannigrahi, J. Sichelschmidt, B. Koo, A. Banerjee, S. Majumdar, and S. Kanungo, J. Phys.: Condens. Matter **31**, 245802 (2019).

[48] B. E. Prasad, S. Sadhukhan, T. C. Hansen, C. Felser, S. Kanungo, and M. Jansen, Phys. Rev. Materials **4**, 024418 (2020).

[49] N. Marzari, A. A. Mostofi, J. R. Yates, I. Souza, and D. Vanderbilt, Rev. Mod. Phys. **84**, 1419 (2012).

[50] D.-T. Chen, J. Chen, X.-G. Li, G. Christou, S. Hill, X.-G. Zhang, and H.-P. Cheng, J. Phys. Chem. C **125**, 11124 (2021).

[51] M. Charlebois, J.-B. Moree, K. Nakamura, Y. Nomura, T. Tadano, Y. Yoshimoto, Y. Yamaji, T. Hasegawa, K. Matsuhira, and M. Imada, Phys. Rev. B **104**, 075153 (2021).

[52] S. Bandyopadhyay, P. Adhikary, T. Das, I. Dasgupta, and T. Saha-Dasgupta, Phys. Rev. B **102**, 220502(R) (2020).

[53] S. Sarkar, S. Kanungo, and T. Saha-Dasgupta, Phys. Rev. B **82**, 235122 (2010).

[54] V. V. Mazurenko, S. L. Skornyakov, A. V. Kozhevnikov, F. Mila, and V. I. Anisimov, Phys. Rev. B **75**, 224408 (2007).

[55] B. Koteswararao, R. Kumar, J. Chakraborty, B.-G. Jeon, A. V. Mahajan, I. Dasgupta, K. H. Kim, and F. C. Chou, J. Phys.: Condens. Matter **25**, 336003 (2013).

[56] T. Saha-Dasgupta and S. Satpathy, J. Phys.: Condens. Matter **15**, 1685 (2003).

[57] T. Saha-Dasgupta, J. Electron Spectrosc. Relat. Phenom. **208**, 83 (2016).

[58] W. M. H. Natori, M. Daghofer, and R. G. Pereira, Phys. Rev. B **96**, 125109 (2017).

[59] G. Jackeli and G. Khaliullin, Phys. Rev. Lett. **102**, 017205 (2009).

[60] S. Steiner, S. Khmelevskyi, M. Marsmann, and G. Kresse, Phys. Rev. B **93**, 224425 (2016).